# Double-clad fiber for endoscopy

**D. Yelin, B. E. Bouma, S. H. Yun, and G. J. Tearney**

*Harvard Medical School, the Wellman Center for Photomedicine, and the Pathology Department, Massachusetts General Hospital,*
*55 Fruit Street, BAR 703, Boston, Massachusetts 02114*

Endoscopes employing a single optical fiber may have advantages over conventional fiber-bundle or CCD array imaging techniques, including the potential for greater flexibility and miniaturization. Although single-mode fibers can provide superior resolution compared with multimode fibers, they are prone to increased speckle noise and suffer from limited optical throughput and reduced depth of field. We demonstrate the use of a double-clad fiber for single-mode illumination and multimode detection to achieve high-resolution, reduced-speckle imaging with high optical throughput and a large depth of field. © 2004 Optical Society of America

*OCIS codes:* 060.2350, 030.6140, 170.2150, 290.5880.

Fiber-optic endoscopy is typically conducted by transmitting an image through a fiber bundle. Although successful for a variety of medical and nonmedical applications, utilization of an array of fibers to form the image imposes constraints on the cost, diameter, and flexibility of the imaging device. As a result, multiple approaches employing a single optical fiber have been proposed[1–7] for miniature, flexible endoscopes. Confocal imaging with a single fiber was implemented by use of the core of a single-mode fiber as both the source and the detection apertures.[1–3] Miniature confocal microscope probes and endoscopes have been constructed by adding a mechanical microscanner at the tip of a single-mode fiber.[4,5] Another single-fiber method for miniature endoscopy, termed spectral encoding, uses a broadband light source and a diffraction grating to spectrally encode reflectance across a transverse line within the sample.[6] A two-dimensional image is formed by slowly scanning this spectrally encoded line and a three-dimensional image may be obtained by placing the probe in the sample arm of an interferometer.[7] In each of the above approaches the core of the single-mode fiber acts as both the source and the detection aperture.

Recently, significant progress has been made in developing high-power fiber lasers utilizing double-clad (also called dual-clad) optical fibers. These fibers are unique in their ability to support single-mode propagation through the core with multimode propagation through the inner cladding. In this Letter we report the use of double-clad optical fiber to obtain reduced-speckle, signal-efficient, spectrally encoded imaging. By coupling the illuminating broadband light into the fiber's core only and collecting the reflected light with the inner cladding, a configuration that we abbreviate as SM-MM, we combine the benefits of single-mode illumination with the advantages of multimode signal collection.

The optical setup for spectrally encoded imaging with a double-clad fiber is shown in Fig. 1. Broadband light from a Kerr-lens mode-locked Ti:Al$_2$O$_3$ laser (750–950 nm) was coupled to the core of a double-clad fiber with a N.A. of 0.4 microscope objective lens. The double-clad fiber (Fibercore Ltd.,

SMM900) had a 3.7-$\mu$m core diameter (4.1-$\mu$m mode-field diameter) with a N.A. of 0.19 and a 90-$\mu$m-diameter cladding with a N.A. of 0.23. The light transmitted from the core was collimated with a 0.4-N.A. microscope objective lens (L0) to approximately a 2-mm beam diameter. We accomplished imaging with single-mode detection and collection (SM-SM) by replacing the double-clad fiber and the beam splitter (BS) with a single-mode 50/50 fiber splitter (Gould Electronics, Inc., Corning HI 780-5/125 fiber, N.A. of 0.14). To simulate a miniature imaging probe, we chose to use a compact lens–grating design in which the beam was first focused by a lens (L1, $f = 65$ mm) and then diffracted by a transmission grating (G1, Holographix LLC, 1000 lines/mm) to form a line on the surface of the sample. A galvanometric optical scanner was used for slow axis scanning.[6] The scattered light was coupled into the inner cladding and the core and deflected by a BS to a spectrometer, which comprised a lens (L2, $f = 40$ mm), a diffraction grating (G2, 1200 lines/mm), and a high-speed line-scan camera (Basler L104k). The images were displayed and stored on a computer. Throughout this work, the power on the sample was approximately 2 mW.

To demonstrate spectrally encoded imaging with the double-clad fiber, we imaged the face of a small doll
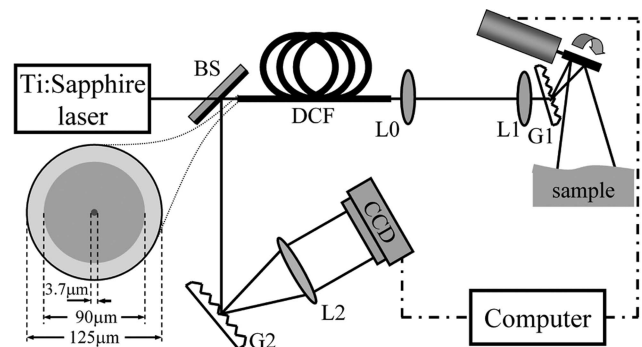


Fig. 1. Schematic of the optical setup for spectrally encoded imaging with double-clad fiber: DCF, double-clad fiber; L0, L1, L2, lenses; G1, G2, diffraction gratings.

© 2004 Optical Society of America

with three different fiber-based illumination-detection configurations: (1) SM-SM (Fig. 2b), (2) SM-MM (Fig. 2c), and (3) multimode illumination with multimode detection with the excitation light coupled mainly to the inner cladding (MM-MM, Fig. 2d). An image of the doll's face with white-light illumination and a CCD camera is presented in Fig. 2a for reference. The SM-SM image (Fig. 2b) had relatively high resolution and contrast but was corrupted by speckle noise. Although the SM-MM image (Fig. 2c) had slightly lower resolution compared with the SM-SM image, its appearance was more natural and more similar to the white-light reference image (Fig. 2a). Also, because of an increase in the depth of field, the doll's neck and shoulder could be seen in the SM-MM image, whereas the small core diameter of the SM-SM image rejected the signal coming from those regions. The MM-MM image (Fig. 2d) did not contain speckle noise and had the largest depth of field but also had a dramatically reduced resolution compared with the SM-SM or SM-MM images. The images that utilized multimode collection, Figs. 2c and 2d, were also much brighter than the SM-SM image.

To gain better understanding of the underlying processes that lead to these results, various imaging parameters, including transverse and axial resolution, collected signal intensity, and speckle contrast, were numerically simulated for different inner-cladding diameters and experimentally measured for the SM-SM and SM-MM configurations. The signal-collection geometry of the double-clad fiber used for the numerical simulations is depicted in Fig. 3a. Grating G1 and the galvanometric scanner were omitted from this illustration for simplicity and to maintain the generality of the scheme. The spatially coherent light (dashed rays) emanated from the core (dark gray on the left) and was focused to a small spot on the sample. Light remitted from the sample can originate from the illuminated spot directly or, in the case of rough surfaces or scattering samples, from locations that are transversely displaced from the focus. Light distributions on the sample were measured with a different setup that included an additional BS, a lens, and a CCD camera placed in the sample arm between the focusing lens and the fiber's tip. The sizes of these light distributions on the samples' surfaces depended on many parameters, such as the wavelength, the sample scattering and absorption properties, polarization, and illumination geometry. However, for all the samples we examined, the measured diameters of the light-scattering distributions were in the range $150-250$ $\mu$m. We therefore considered a light-scattering distribution of 200 $\mu$m as representative for typical samples of interest and in turn utilized this value for our simulations. In the simulation the scattered light (dotted lines in Fig. 3a) was imaged back onto the face of the fiber and coupled mainly into the inner cladding (lighter gray).

For the point-spread function calculations we treated the double-clad fiber as a confocal imaging system in which the inner cladding was simulated by a finite-sized pinhole, thereby establishing a correspondence between our results and previously

published confocal microscopy calculations.[8] Because of the finite N.A. and discrete nature of the number of propagating modes in the inner cladding, the validity of this approximation depends on the specific fiber parameters. For example, a 6-$\mu$m-diameter, 0.23-N.A. core supports 12 propagation modes at
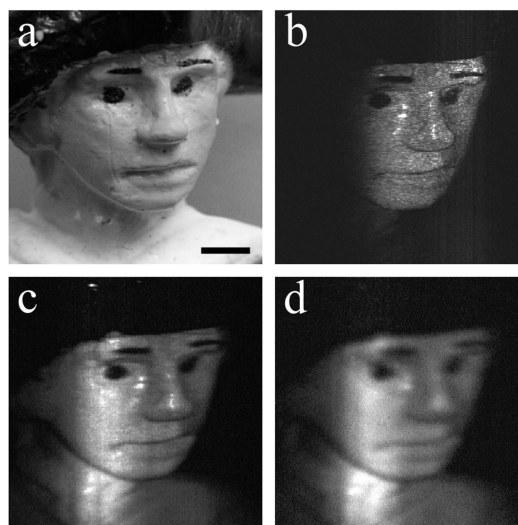


Fig. 2. a, Standard white-light image of the face of a doll. The scale bar represents 2 mm. Spectrally encoded imaging of the face of a doll with the following configurations: b, SM-SM; c, SM-MM; d, MM-MM.
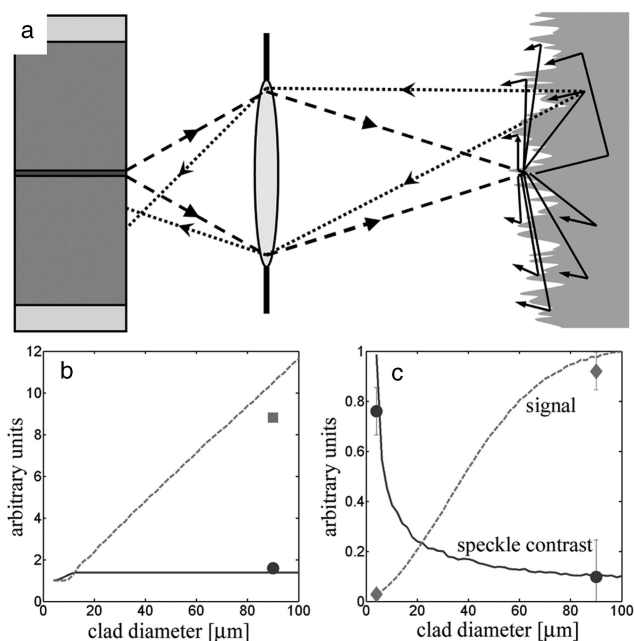


Fig. 3. a, Signal collection with the double-clad fiber. The lens images the scattered light on the face of the inner cladding. b, Normalized SM-MM transverse (solid curve, simulation; filled circle, measurement) and axial (dashed curve, simulation; filled square, measurement) spot sizes plotted as a function of inner-cladding diameter. c, Speckle contrast (solid curve, simulation; filled circle, measurement) and normalized total signal intensity (dashed curve, simulation; filled diamond, measurement). All the SM-MM values are normalized to those of the SM-SM case. Error bars represent 1 standard deviation.

a wavelength of 0.85 $\mu$m. This number increases proportionally to the guiding area, and, as a result, for the SMM900 fiber (90-$\mu$m-diameter inner cladding) we would expect nearly 3000 modes to be guided. We therefore expected the pinhole model to correspond to experimental measurements. By numerically solving the Fresnel integral, we calculated the FWHM of the point-spread function.[8] The transverse and the axial spot sizes, normalized to unity when the cladding diameter was equal to the core diameter, are shown as solid and dashed curves, respectively, in Fig. 3b. The transverse spot size increased by up to a factor of 1.4 and then remained constant for large cladding diameters, whereas the axial spot increased almost linearly. We estimated the transverse point-spread function by taking the derivative of the signal from an edge in a standard resolution chart. The FWHM of the measured line-spread function was $17.4 \pm 1.5$ $\mu$m with the SM-SM configuration (the mean of 35 locations on the image) and $27.7 \pm 2.9$ $\mu$m for the SM-MM case (shown by a filled circle in Fig. 3b). The FWHM of the measured signal obtained by scanning a mirror along the optical axis through the focal point, was measured for the SM-SM and SM-MM configurations to be approximately $2.1 \pm 0.3$ and $18.5 \pm 3$ mm, respectively. The ratio between these measurements was 8.8 (shown by a filled square), which was slightly lower than the ratio of 10.5 obtained from our simulation.

Efficient signal collection is important for high signal-to-noise ratio imaging. We calculated the detected signal intensity by simulating 1000 rough surfaces (one random surface for each point on the sample) with uniformly distributed random amplitude and phase, within a Gaussian intensity envelope of 200-$\mu$m FWHM. We calculated the light distribution at the tip of the fiber by convolving the image predicted by geometric optics with an impulse response that is the Fraunhofer diffraction pattern of the lens pupil.[9] The normalized total signal intensity that was collected with the inner cladding is plotted in Fig. 3c as a dashed curve. For small cladding diameters the signal collection increased with the cladding area. The total collected signal reached a plateau as the cladding covered the entire extent of the scattered light. We measured the total signal from a highly scattering paper at the object plane and found that the signal collected with the SMM900 inner cladding was 32.5 times stronger than the signal that was collected in the SM-SM case (diamonds in Fig. 3c). This measurement was in good agreement with the ratio of 35 obtained from our simulation.

Speckle noise is one of the limiting factors in many coherent imaging techniques. It reduces the effective resolution, produces image artifacts, and makes images look unnatural. Using the simulation described above for the detected signal intensity, we calculated the speckle noise by dividing the standard deviation of the image by its mean.[10] The resulting speckle contrast, plotted as a solid curve in Fig. 3c, rapidly decreases with the increasing cladding diameter. We measured the speckle contrast for 50 lines of an image of a rough aluminum surface. For the SM-SM

configuration we measured the speckle contrast to be $0.76 \pm 0.09$, and for the SM-MM case we measured a speckle contrast of $0.1 \pm 0.15$ (shown as filled circles in the plot), corresponding to a reduction of speckle by a factor of 7.6. This ratio was in good agreement with that of our simulation, which demonstrated a ratio of 9.4.

These experiments and simulations show the benefits of the SM-MM configuration for single-fiber endoscopy. As expected, when the diameter of the inner cladding was equal to the diameter of the core (SM-SM), our results demonstrated spatially coherent or confocal behavior. The images in this case had the highest resolution and contrast but suffered from speckle noise, low signal power, and a relatively limited depth of field. The SM-MM configuration provided by the double-clad fiber is analogous to opening the pinhole in a free-space confocal microscope.[8] The large area of the cladding improved the detection efficiency, increased the depth of field, and decreased speckle noise, resulting in natural-appearing images.

In summary, we have shown that the use of a double-clad optical fiber provides many benefits to single-optical-fiber-based endoscopic imaging. In the future we plan to incorporate a double-clad fiber into an ultraminiature endoscope probe with a miniature lens and grating, in which the slow-axis scan could be performed, for example, by spinning the probe. Double-clad optical fibers can be used to enhance several other fiber-based imaging and nonimaging systems. In particular, systems that do not need coherent signal detection, such as fluorescence and Raman, would benefit from the increase in signal and depth of field.

## References

1. T. Dabbs and M. Glass, Appl. Opt. **31,** 3030 (1992).
2. P. M. Delaney, M. R. Harris, and R. G. King, Appl. Opt. **33,** 573 (1994).
3. R. Juskaitis and T. Wilson, Opt. Lett. **19,** 1906 (1994).
4. D. L. Dickensheets and G. S. Kino, Opt. Lett. **21,** 764 (1996).
5. E. J. Seibel and Q. Y. J. Smithwick, Lasers Surg. Med. **30,** 177 (2002).
6. G. J. Tearney, M. Shishkov, and B. E. Bouma, Opt. Lett. **27,** 412 (2002).
7. D. Yelin, B. E. Bouma, N. Iftimia, and G. J. Tearney, Opt. Lett. **28,** 2321 (2003).
8. T. Wilson and A. R. Carlini, Opt. Lett. **12,** 227 (1987).
9. J. W. Goodman, *Introduction to Fourier Optics* (McGraw-Hill, New York, 1996).
10. J. C. Dainty, *Laser Speckle and Related Phenomena* (Springer-Verlag, New York, 1984).